ORIGINAL PAPER

Check for updates

Crude dry extract from *Colocasia esculenta* in association with poly(vinyl alcohol) as biomaterial to prepare bioactive wound dressing

Elisabeth Maria López de Prado[1] · **Geanne Aparecida de Paula**[2] ·
Jessyca Aparecida Paes Dutra[3] · **Daniel Fernandes Cipriano**[4] ·
Rodrigo Rezende Kitagawa[3] · **Fabiana Dayse Magalhães Siman**[2] ·
Eduardo Frizzera Meira[2] · **Jair Carlos Checon de Freitas**[4] ·
Juliana Aparecida Severi[2] · **Lílian Gasparelli Carreira**[6] ·
Rodrigo Lamberti Oréfice[5] · **Janaina Cecília Oliveira Villanova**[1,2,3]

Abstract

Colocasia esculenta (taro) is traditionally reported to be rich in bioactive compounds with pharmacological properties, and it is a source of starch—a natural polymer with film-forming capacity. The present work aimed to use the crude dry extract from taro rhizome in high proportions to form polymeric films in association with PVA, for use as biomaterials to prepare wound dressing. The films prepared by solvent casting technique were analyzed to evaluate their physicochemical parameters, barrier, and mechanical properties, and in vitro biocompatibility, important attributes for the functionality and safety of films for wound dressing application. The starch contained in the taro extract showed good filmogenic properties after prior

✉ Janaina Cecília Oliveira Villanova
pharmacotecnica@yahoo.com.br

1 Programa de Pós-graduação em Ciências Veterinárias, Universidade Federal do Espírito Santo - UFES, Alegre 29500-000, Brazil

2 Laboratório de Desenvolvimento de Produtos Farmacêuticos - LDPF, Universidade Federal do Espírito Santo - UFES, Av. Alto Universitário, sem número, Guararema, Alegre 29500-000, Brazil

3 Programa de Pós-graduação em Ciências Farmacêuticas, Universidade Federal do Espírito Santo - UFES, Vitória 9043-900, Brazil

4 Laboratório de Materiais Carbonosos e Cerâmicos - LMC, Universidade Federal do Espírito Santo - UFES, Vitória 9043-900, Brazil

5 Laboratório de Engenharia de Polímeros e Compósitos - LEPCom, Universidade Federal de Minas Gerais - UFMG, Belo Horizonte 31270-901, Brazil

6 Departamento de Engenharia Rural, Universidade Federal do Espírito Santo – UFES, Alegre 29500-000, Brazil

gelatinization in water and then blending with the PVA solution containing glycerol. Moreover, the films obtained were thin, smooth, transparent, shiny, and domain-free. SEM photomicrographs showed the existence of a continuous and homogeneous microstructure. Additionally, the blends were partially miscible and presented an altered crystalline structure. The thermal stability and mechanical resistance parameters were improved due to the presence of the taro extract. In addition, the parameters pertaining to the functionality of the films as wound dressings were improved, particularly in the films containing higher proportions of the extract, which is configured as an advantage, since the taro extract proved to be non-cytotoxic, biocompatible, with healing activity, and it comes from a renewable source. Crude extract from taro rhizome blended with PVA proved to be suitable for the intended purpose.

Graphical abstract
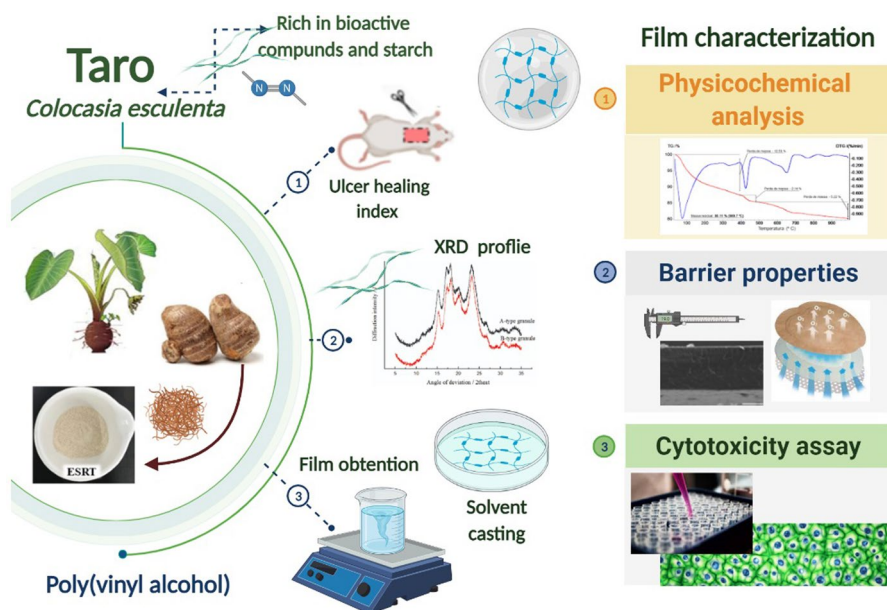
Introduction

In recent decades, there has been a growing demand from society for products derived from natural and renewable sources, in response to a great concern worldwide about the environment and the possibility of scarcity of non-renewable resources. Thus, people's consumption habits are changing, and options to consume "environment friendly" alternative products are increasing [1–3]. Plant-derived

biomaterials are a great promise in actuality to harness the bioactivity, biocompatibility, and biodegradability superior properties of these materials and the possibility to reduce the biowaste disposition in nature. These materials are ecologically safe and can be derived from plenty of agricultural food resources and various biodegradable waste materials which reduce their synthesis and processing cost [4, 5]. In this scenario, the use of amylaceous polysaccharides has gained prominence, especially in the food and pharmaceutical industries due to its ability to form edible and non-edible films for food packaging and drug delivery systems [6–9].

Plants for food use are a rich source of carbohydrates and bioactive phytochemicals [7–9]. Brazil has a great variety of endemic roots, tubercles, and rhizomes, such as taro (*Colocasia esculenta* L. Schott), belonging to the family Araceae. Taro is an herbaceous plant, originally from Asia, that grows in tropical and subtropical regions; the rhizomes of this plant are edible and are considered a low-cost food with high nutritional value, containing carbohydrates, proteins, vitamins, minerals, lipids, and phenolic compounds [10, 11]. This plant contains an average of 16–24% of starch that can reach 80% or more of dry mass and could represent an alternative source of starch. In addition to the high content of starch polysaccharides, taro rhizomes contain up to 25% mucilages with high fluid retention capacity, exhibiting humectant and protective action beneficial for healing [12]. Moreover, immunostimulant polysaccharides and defense proteins have been isolated from taro rhizomes. Additionally, studies have shown the presence of polyphenols in taro, particularly flavonoids as bioactive compounds with a marked antioxidant [13–16]. Therefore, taro rhizomes and leaves have been traditionally used as wound healer, and in vitro studies and research on animal models have demonstrated the antioxidant, immunomodulatory, and healing properties of taro [14, 16–18].

The most common sources of native starch are grains (corn, rice, and wheat) and rhizomes and tubers (potato, sweet potato, yam, and cassava). Less conventional sources are sago, chickpea, quinoa, mango, banana, mandioquinha, and taro [19]. Native starch can be easily extracted in water, which is the most abundant solvent and harmless to the environment and human and animal health [20, 21]. Starch is in the form of water-insoluble granules, which hydrate and produce low-viscosity colloidal dispersions [22]. According to many studies, starch from potato, cassava, corn, and yam is a promising polymer for film preparation due to its high amylose content, which is responsible for the production of strong and flexible films. In the present study, we investigated the possibility of using the crude aqueous extract of taro rhizome, rich in starch containing 19% amylose, in the preparation of films [23, 24].

Starch is an attractive material for preparing bioactive wound dressings owing to its high biocompatibility and good healing properties, as reported in the literature [25]. In addition, the ability of starch to biodegrade and reduce environmental pollution, easy availability of natural sources of starch, which makes it a low-cost material, and the ease of processing using conventional equipment, justify its use [4, 5]. Moreover, starch films are odorless, tasteless, colorless, non-toxic, absorbable, and semipermeable to gases and moisture [22]. To overcome the limitations associated with the use of natural polymers in the preparation of films, such as rapid dissolution, poor barrier properties, and low mechanical resistance, especially in humid

environment, the blend containing natural and synthetic polymers is a promising alternative. To form polymeric blends is a low-cost option to optimize the performance and functionality of the isolated polymers [4, 21]

The use of starch obtained from the taro rhizomes as pharmaceutical excipients to use as binder, disintegrant and matrix former in tablets formulations were related [8, 26–29]. Wardhani et al. [30] prepared films by electrospinning proteins isolated from taro rhizomes, poly(ethylene oxide), and chitosan, crosslinked by heat or glutaraldehyde vapor. Morphological cell analysis revealed that fibers containing 2% w/v taro proteins increased cellular proliferation, and therefore, enhanced the potential for use in wound dressing. However, there are no reports on the use of crude extract of taro rhizome in the preparation of polymeric films for pharmaceutical purposes. The objective of the present work was to use the crude extract from taro rhizome as a natural source of bioactive compounds and starch to form polymeric films in association with PVA, for use as biomaterials to prepare wound dressings. Crude dry extract from taro rhizome (ESRT) was obtained by initial extraction in purified water, followed by lyophilization. Subsequently, in vivo studies were performed to validate non-cytotoxicity and healing activity of the extract. Films were prepared by solvent casting technique using poly(vinyl alcohol) (PVA) in the proportions 100:00, 90:10, 80:20, 70:30, and 60:40% w/w (PVA/ESRT), after determining the crystalline fraction of the starch present in ESRT. The films were subjected to different tests to validate their applicability as wound dressings, such as cytotoxicity and biocompatibility tests in vitro; evaluation of the composition, miscibility, compatibility, and stability; and determination of the mechanical resistance and barrier properties.

Materials and methods

Materials

PVA with an average molar mass of 85,000–124,000 and high degree of hydrolysis (+99%), pH 7.4 saline-phosphate buffer (SPB), and citrate-dextrose acid solution (ACD) were purchased from Sigma-Aldrich (USA). Dulbecco's modified Eagle's medium (DMEM) and fetal bovine serum (FBS) were obtained from Vitrocell (Brazil). Dimethyl sulfoxide (DMSO); sodium carboxymethylcellulose (CMC-Na), pharmaceutical grade; vegetable glycerol, USP grade; sterile saline solution, (0.9% w/v); Concreta® marigold ointment (Simões Laboratory; MS registration 1.0576.0004.001–5); 10% w/v injectable ketamine solution; and 2% w/v injectable xylazine solution (Syntec Laboratory) were purchased from local suppliers.

Preparation of crude dry extract of taro rhizomes

To prepare the extract in dry powder form, 300 g of fresh and peeled rhizomes was weighed, 300 ml of deionized water was added, and the mixture was left to stand for 10 min. The mixture was then subjected to turbolysis for 5 min. The aqueous

extract thus obtained was filtered, and the extracted solution obtained was frozen in a freezer at $-20\ °C$ for lyophilization (Liotop, L100, Brazil).

Determination of the crystalline fraction in the ESRT by X-ray diffraction (XRD)

The XRD pattern of the ESRT powder sample was recorded at room temperature using a Shimadzu X-ray diffractometer (XRD-6000, Japan), operating at 40 kV and 30 mA, with Cu-Kα radiation ($\lambda = 1.5418$ Å). The diffraction angle (2θ) was varied from 5° to 70° with a step size of 0.02° and at a scan rate of $0.50°\text{min}^{-1}$.

In vivo evaluation of the healing activity of ESRT

In vivo test was carried out after approval by the *Ethics Committee on the Use of Animals* (ECUA-UFES, approval number 006/2019), using methodology adapted from Caetano, Frade, Minatel, Santana, and Enwemeka [31], Garros et al. [32], Koga, Pereira, Lipinski, and Oliveira [33], and Zonari et al. [34]. Adult male Wistar rats ($n = 45$) used in the study were supplied by the vivarium of the Health Sciences Center of the Federal University of Espírito Santo (UFES). The animals were randomly assigned to three groups ($n = 15$), as follows: group 1—negative control: animals treated with 0.9% w/v saline (group C−); group 2—positive control: animals treated with Concreta® marigold ointment (group C+); and group 3—animals treated with the ESRT suspended in the inert vehicle, at a concentration of 400 mg ml^{-1} (group ESRT). To induce excision of lesions in animals, they were anesthetized with intraperitoneal ketamine (91 mg kg^{-1}) and xylazine (9.1 mg kg^{-1}). Next, each animal was placed in the prone position on an acrylic board, subjected to trichotomy in the dorsal region of the chest, and lesions were induced. A rectangular mold (1.5×2 cm) was used to delimit the incision area, which was made using surgical scissors. A fragment was removed from the craniocaudal region, exposing the dorsal muscle fascia, consisting of the skin and subcutaneous tissue. The surgical procedure was performed using aseptic technique.

Healing activity was determined by macroscopic observation of the wound area and by determining the ulcer healing rate. The rats were sedated with xylazine intraperitoneally (10 mg kg^{-1}) to assure relaxation of the muscles and standard animals' position in the records, while taking photographs and measuring the area of the lesions. The lesions were photographed using a digital camera (Sony, Cyber-shot 8.1 megapixels), kept on a tripod at a fixed distance of 38.5 cm. Images were obtained with pixel dimensions of 3264×2448 pixels in the JPG file format with file size of 2.5 MB. The area of each lesion was measured three times (mean value was considered for calculations) by digital planimetry using image analysis software (ImageJ). The contraction of the wound area of each animal was determined by calculating the ulcer healing index (UHI) using Eq. 1, where ALT is the area of the lesion at the time of evaluation and ALI is the initial area of the lesion. The experimental data were subjected to one-way analysis of variance and Bonferroni test ($p < 0.05$).

$$\text{UHI} = \frac{\text{ALI} - \text{ALT}}{\text{ALI}} \qquad (1)$$

Preparation of polymeric blends and films

PVA dispersion was prepared at a concentration of 8% w/v in deionized water using a mechanical stirrer (Fisatom, model 713D, Brazil) at 350 rpm and temperature between 90 and 100 °C until complete polymer solubilization. The dispersion of ESRT (2.5% w/v) in deionized water was prepared using a mechanical stirrer (Fisatom, model 713D, Brazil) at 350 rpm, with a gradual increase in temperature up to 85 °C, for 40 min, until gelatinization of the starch present in the extract. Glycerol (1% w/v) was added in each dispersion after cooling. To obtain the blends, different proportions of the polymeric dispersions (PVA/ESRT; 100:0, 90:10, 80:20, 70:30, and 60:40% w/w) were mixed using magnetic stirring (Fisatom, model 753A, Brazil) for 60 min.

The films were prepared by the solvent casting technique by depositing 10 g of each blend on glass plates with a standardized diameter (9 cm), which were left exposed to the air for 72 h, until complete drying. After drying, the films were removed from the plates with the aid of tweezers and stored in airtight plastic bags.

Physicochemical characterization of films

Scanning electronic microscopy (SEM)

The morphology of the cross-sections of the films was studied by scanning electron microscopy (SEM) using Jeol equipment (JEM-6610LV, Japan) at an acceleration voltage of 20 kV, with a magnification of 500 and 1000×. The samples were coated with gold using a metallizer (Desk V, Denton Vacuum, United States). The cross sections of the films were obtained by cryogenic fracturing process (immersion in liquid nitrogen, followed by shock).

Fourier transform infrared spectroscopy (FTIR)

The composition of the ESRT and the films was evaluated by infrared analysis using Fourier transform (BRUKER, Tensor 27, USA). Data acquisition was performed with 64 scans, between 4000 and 600 cm^{-1}, in an ATR accessory (Attenuated Total Reflectance) using zinc selenide (ZnSe) crystal.

X-ray diffraction

The XRD patterns of the film samples were recorded at room temperature using Rigaku Miniflex 600-C X-ray diffractometer, operating at 40 kV and 15 mA, with Cu-Kα radiation ($\lambda = 1.5418$ Å). The diffraction angle (2θ) was varied from 5° to 90° with a step size of 0.05° and at a scan rate of 10°min^{-1}.

Thermal analysis

DSC measurements were performed using Exstar equipment (model DSC7020, Japan) in aluminum pans under N_2 atmosphere with a flow rate of 50 ml min^{-1} and a heating rate of 10 °C min^{-1}. Initially, the sample was heated from 25 to 200 °C, followed by cooling to 0 °C, and reheated to 200 °C; TG/DTG thermograms were obtained using an Exstar thermobalance (model 7200, Japan), between 25 and 800 °C, under an inert N_2 atmosphere at a heating rate of 10 °C min^{-1}.

Study of the barrier properties of the films

The films were subjected to different tests to study their barrier properties. All measurements were performed in triplicate, and the results were expressed as the mean ± standard deviation (SD).

The wettability of the films was evaluated by the sessile drop method, using a GBX goniometer (Digidrop-DI, Ireland) to measure the contact angle (φ) formed between the samples and 5 μl of phosphate-buffered saline (SPB) (pH = 7.4) deposited on their surface, at 25 ± 2 °C. The results represent the average angle between the tangent line and the surface of the films, referring to the right and left sides of the deposited drops. Ten consecutive measurements were performed at room temperature using the surface energy mode of the software. The parameters such as work of adhesion and spreadability were calculated directly.

The thickness was evaluated using a digital micrometer (Mitutoyo, 293–230, Brazil) at randomly selected five points for each film (three peripherals and two central).

The swelling index was determined according to the method described by Xie et al. [35]. Films with dimensions of 2 × 2 cm were initially dried in an oven (Steriler, SX1.3DTME, Brazil) at 105 °C for mass normalization, and they were then placed in a beaker containing 50 ml of SPB solution (pH = 7.4) at room temperature. After 60 min, the films were collected with tweezers, the excess liquid was removed with absorbent paper, and the films were weighed again. The swelling index (Q%) represents the increase in the mass of the films and was calculated using Eq. 2, where *ms* and *md* are the weights of the swollen and dry films, respectively.

The solubility of the films was determined using a method described by Flores, Costa, Yamashita, Gerschenson, and Grossmann [36] for mass loss assessment: films with and without extract (2 × 2 cm) were dried in an oven at 105° C for mass normalization, weighed, and placed in Erlenmeyer flasks containing 50 ml of SPB solution (pH = 7.4). The flasks were shaken in a reciprocating bath (Marconi, model MA93, Brazil) at room temperature for 48 h. The solubility index represents the amount of mass lost (ML%) for each film and was calculated using Eq. 3, where *mf* and *mi* are the final and initial masses of the film, respectively.

$$Q\% = \frac{\mathrm{ms} - \mathrm{md}}{\mathrm{md}} \times 100 \qquad (2)$$

$$ML\% = \frac{mi - mf}{mi} \times 100 \qquad (3)$$

To determine the water vapor permeability rate (WVPR), a modified "cup" gravimetric method was used [37]. A sample of each film of standardized diameter was firmly attached to the top of the cup containing 9 g of anhydrous calcium chloride as a desiccant. The cup was then placed in a climatic chamber (Shellab, HC9R2, Brazil) at 25 °C and 75% relative humidity (RH) for 48 h. The weight of the desiccant was periodically measured to assess the weight gain. The results were calculated using Eq. 4, in which WVPR is the water vapor permeability rate ($gm^{-2} d^{-1}$), Δm is the mass of water absorbed by the hygroscopic material at time "t" (g), Δt is the permeation time (days), and A is the exposed area of the specimen (m^2). All measurements were performed in triplicate, and the results are expressed as the mean $\pm$ SD.

$$WVPR = \frac{\Delta m}{\Delta t} \cdot \frac{1}{A} \qquad (4)$$

The residual moisture content of the films was determined using a Shimadzu infrared moisture analyzer (model MOC63u, Japan). Films (2×2 cm) were placed on the scale plate and heated to 105 °C until a constant mass was achieved. The values of the mass, percentage of moisture, and time required to achieve constant mass were obtained automatically.

Mechanical resistance

The mechanical properties of the films were determined from the stress–strain curve obtained by a universal testing machine (EMIC/Instron, model DL-3000, Brazil) in tensile mode, with 50 N force cell capacity and a strain or deformation rate of 10 mm/min. The tests were carried out according to the ASTM standard D638.

In vitro preliminary biocompatibility study

The preliminary biocompatibility was assessed by determining the hemolytic index (HI) as follows: samples of the films (1×1 cm) were inserted in Eppendorf microtubes containing 0.9 ml of blood and 0.1 ml of ACD. The microtubes were incubated in a water bath (Fanem 1100, Brazil) at 37 °C for 3 h. The tubes were gently inverted twice every 30 min to ensure contact between the films and blood. After incubation, the microtubes were centrifuged at 3000 rpm for 20 min using a centrifuge (Hettich Mikro 200, Germany). The supernatants were transferred to a 96-well plate and the absorbance was measured using an ultraviolet–visible (UV–Vis) spectrometer (Thermo Fisher, Multiskan GO, Finland) at 540 nm. Purified water and SPB were used as positive and negative controls, respectively. Tests were performed in triplicate. The hemolysis percentage was calculated using Eq. 5, where A_{sample}, $A_{negative\ Control}$, and $A_{positive\ Control}$ are the absorbance values of the film, negative control, and positive control, respectively. The results were expressed as the mean $\pm$ SD.

$$HI = \frac{(A\ sample - A\ negative\ control)}{(A\ positive\ control - \ control)} \quad (5)$$

The cell viability assay was performed in murine macrophages cell line RAW 264.7 (ATCC TIB-71), which was obtained from the Cell Bank of Rio de Janeiro, Brazil (BCRJ). The cells were cultured in DMEM supplemented with 10% FBS and incubated at 37 °C and 5% CO_2 until attainment of 70–90% confluence. The macrophages were dissociated using a cell scraper and counted in a Neubauer chamber. Aliquots (0.2 ml) of the cell suspension containing 50×10^5 cells.ml^{-1} were transferred to 96-well plates. Then, the plates were incubated in a modified atmosphere (37 °C, 5% CO_2) for 24 h for adherence. After this period, the medium was obtained and the cells were treated with modified medium containing ESRT alone or with the films (0.125–8 mgml^{-1}). The plates were incubated for 24 h under the same conditions. After treatment, viability was evaluated using the MTT-tetrazolium method [38]. Unmodified medium (baseline group) and 4% DMSO were used as controls to evaluate the effectiveness of the assay. Cell viability was determined against the baseline group considered as 100% growth. The tests were performed in triplicate, with three repetitions. The variation in viability was statistically compared using the two-way analysis of variance (ANOVA), followed by the Bonferroni post-test.

Results and discussion

Preparation of the ESRT and measurement of crystallinity by XRD

An aqueous extraction was performed with 300 g of fresh rhizomes and 300 ml of deionized water, which yielded 485 g of aqueous extract and finally 63.8 g of dry taro rhizome extract, with a yield of 21.3% of the mass of fresh rhizomes. The dry extract was granular with slightly rose color (Fig. 1) and was stored in an airtight container.

Turbolysis is an extraction technique that involves the rupture of cellular tissues by strong agitation, resulting in release and extraction of the substances of interest
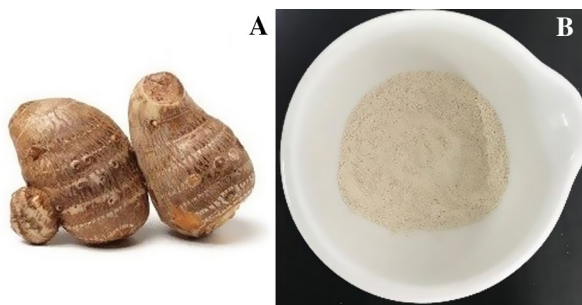

Fig. 1 Taro rhizomes (**A**) and crude dry extract from taro rhizomes (**B**) obtained from the aqueous dispersion by turbolysis followed by lyophilization

present in the plant material. In addition, this method is similar to the preparation of plasters or compresses for wound healing based on the ethnopharmacological use of rhizomes [18]. Advantages in the use of water as solvent for extraction includes: reduced environmental impact, selective extraction, no hazards, faster start-up, and simplification of process steps [39]. Moreover, lyophilization effectively removes water to promote the chemical and microbiological stability of the material, and to maintain the chemical integrity of its components [40]. Turbolysis as the extraction process and water as the extracting solvent followed by filtration and freeze-drying of the crude extract was preferred to maintain the integrity of all components of interest for the healing action and for the formation of the film. After preparing the extract, the presence of starch and its crystalline fraction were investigated by XRD. The diffraction profile of the ESRT sample is shown in Fig. 2.

The main diffraction peaks observed at 2θ in the present study were at $15.1°$, $17°$, $18°$, and $23°$, which are characteristic of type A starch [41]. Besides overlapping peaks, a wide background visible in the diffractogram might be attributed to the amorphous fraction of the starch and other compounds present in the ESRT owing to the absence of selective extraction for native starch. The A-type crystalline starch is obtained from cereals and shows intensity peaks at 2θ diffraction angles at approximately $15.3°$, $17.1°$, $18.2°$, and $23.5°$; B-type starch from fruits, rhizomes, and tubers, shows peaks at approximately $5.6°$, $14.4°$, $17.2°$, $22.2°$, and $24°$; and C-type from vegetables and roots, at approximately $5.6°$, $15.3°$, $17.3°$, and $23.5°$ [42].

Starch granules have varying content of amylose and amylopectin. Amylose is largely linear formed by glucose units linked by α-1,4 bonds and has an excellent ability to form films. On the contrary, amylopectin is a highly branched material formed by short chains connected by α-1,4 bonds, with branching points occurring every 25–30 glucose units and connected by α-1,6 bonds [43]. The molecular weight of amylose is approximately 10 times greater than that of conventional synthetic polymers, such as polyethylene, polypropylene, and polystyrene [4, 44, 45]. The latter,
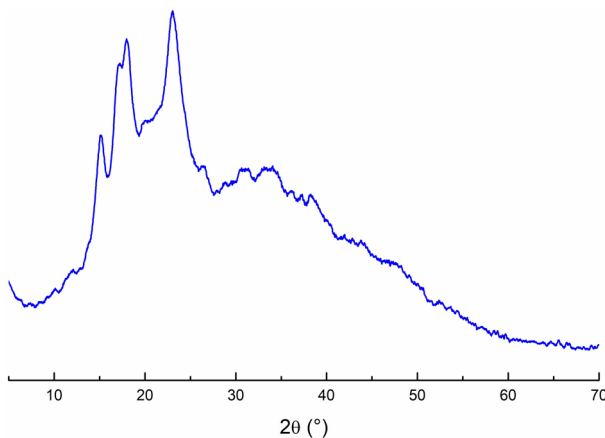

Fig. 2 X-ray diffractogram of ESRT

together with the amylopectin branch points, represent the amorphous fraction of starch, whereas the crystalline fraction is represented by the short-branched chains of amylose. Therefore, the more the amylose content in starch, the greater is the crystallinity of the polymer [5, 46]. High amylose corn starch is known to produce strong and flexible films [47].

The degree of crystallinity of starch was estimated by analyzing the peaks at 2θ region typically associated with starch and by applying a deconvolution method, which allowed the separation of the contributions due to the amorphous and crystalline fractions of the starch [48–50]. In the present study, the degree of crystallinity for the starch present in the ESRT was calculated as 19%. Most native starch has approximately 1445% crystallinity [48, 51]. Aboubakar et al. [52] found an amylose content of approximately 25% in taro starch. Slightly lower value found in the present study could be explained by the presence of other components in the ESRT, in contrast to extraction of only starch from rhizomes, tubers, or grains in other studies [23, 53]. Wang et al. [41] obtained 17.12% amylose content in taro starch. Nevertheless, the variations observed in the amylose content of different starch might be attributable to soil, climatic conditions, and the different procedures used for the isolation of starch [54].

Evaluation of the healing activity of ESRT

Taro rhizomes are rich in starch polysaccharides and other components, such as immunomodulatory proteins, mineral salts, vitamins, and other bioactive compounds of healing interest [15, 17, 55]. Due to the presence of these components, taro rhizomes have been popularly used for wound healing in the form of compresses containing freshly grated rhizomes, which are applied directly to wounds [18, 56]. Macroscopic observation of the wounds induced in rats and treated with ESRT showed progressive closure of the lesions over time, with absence of necrosis and secretion in all treatment groups. Table 1 shows the values obtained for the ulcer healing index at 0, 7, 14, and 21 days after lesion induction. The means followed by the same letters in the lines do not differ according to the Bonferroni test, at 5% probability.

Considering the UHI values obtained, it can be observed that after 7 days, there was a significant difference ($p < 0.05$) between the values of the commercial

Table 1 Ulcer healing index indicative of the healing effect of ESRT

Time (days)	Treatment		
	C−	C+	ESRT
0	0.000 ($\pm$0.000)[a]	0.000 ($\pm$0.000)[a]	0.000 ($\pm$0.000)[a]
7	0.459 ($\pm$0.034)[b]	0.579 ($\pm$0.030)[a]	0.405 ($\pm$0.029)[b]
14	0.819 ($\pm$0.018)[b]	0.909 ($\pm$0.013)[a]	0.880 ($\pm$0.012)[a]
21	0.955 ($\pm$0.016)[a]	0.988 ($\pm$0.009)[a]	0.982 ($\pm$0.009)[a]

Different letters (a and b) show statistical difference ($p < 0.05$)(vertical lines); n = 3

formulation (C+) group and those of other groups (animals treated with saline and ESRT). However, there was no significant difference between the ESRT and C+ groups ($p < 0.05$) after 14 days, while there was a significant difference ($p < 0.05$) between the UHI values of the C- and ESRT groups. Moreover, after 21 days, there was no significant difference ($p < 0.05$) between the groups tested; however, after 14 and 21 days, higher UHI values were observed for the treatment groups C+ and ESRT.

The values of the ulcer healing index have been interpreted as follows: UHI < 0 represented an increase in the lesion area, UHI > 0 represented a decrease in the lesion area, and UHI = 1 represented the total closure of the lesion [31]. In the present study, the maximum change in the UHI values occurred after 7 days of lesion induction. There was no significant difference in the UHI value on days 14 and 21 for the animals treated with either commercial formulation or ESRT, and the UHI value approached 1 on day 21, indicating almost complete closure of the lesions. Notably, there was complete closure of the lesions in two animals in the C+ group and in one animal in the group treated with ESRT, after 21 days. These findings suggest that ESRT has healing activity similar to that observed for the commercially available formulation under current experimental conditions; the pharmacological action of ESRT accompanied by the presence of the components that have ability to form films justifies its incorporation in films.

Preparation and physicochemical characterization of films

Blends of PVA and starch have been studied for several purposes, including good biodegradability and film formation ability of the final material [57]. Native starch or its standardized pure components have been used for the preparation of films by different methods, such as a colloidal dispersion or an emulsion of starch in excess quantity of water, usually above 90% [58, 59]. Starch granules are insoluble in cold water due to occurrence of strong hydrogen bonds between the chains under this condition. However, upon heating, the structure of the crystalline fraction is interrupted, and the water molecules interact with the hydroxyl groups of amylose and amylopectin, resulting in partial solubilization of starch [60, 61]. The heating of starch dispersions in excess quantity of water and at high temperatures (between 65 and 100 °C) causes the starch chains to break down, leading to a phenomenon called gelatinization. Gelatinization occurs in two stages (hydration and diffusion of the solvent in the starch granules followed by their fusion) with irreversible structural changes, and water absorption, swelling, and loss of crystallinity [62, 63].

In the present study, gelatinization of the starch in ESRT dispersion (2.5% w/v) was obtained by slow increase in temperature to 85 °C for 40 min, a method adapted from Araujo-Farro, Podadera, Sobral, and Menegalli [64] for the preparation of quinoa starch films. A viscous, opaque dispersion was obtained, which was mixed with the PVA dispersion (8% w/v) in different proportions. The use of a plasticizer (glycerol; 1% w/w) makes the film more flexible and extensible because it reduces intermolecular forces and increases the mobility of polymer chains [57, 65]. However, plasticizers can increase the permeability of the films

to moisture, oxygen, and aromatic compounds, modifying their barrier properties [66, 67]. An effective plasticizer, such as glycerol is one of the most used plasticizers owing to its compatibility with the polymeric matrix [5] and high capacity to form hydrogen bonds with water, maintaining moderate humidity in the films [22]. Visually, the dispersions were miscible and transparent.

The composition, presence of interactions, structural organization, miscibility, compatibility, and stability in the films were analyzed using different techniques, namely SEM, FTIR-ATR, XRD, DSC, and TG/DTG. Photograph and photomicrograph images of the films are shown in Fig. 3. The dispersion of plasticized pure extract resulted in a fragile and brittle film, which did not resist handling. The PVA films plasticized by glycerol and those obtained from the blends were
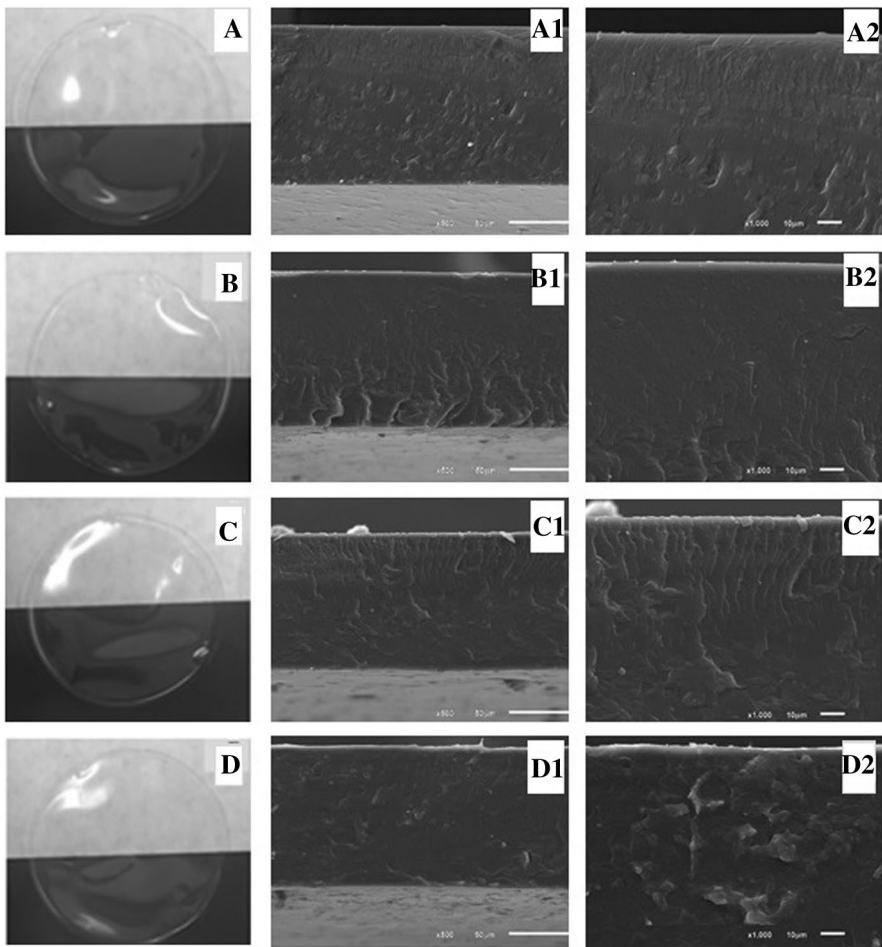

Fig. 3 Photo images of the films (**A**, **B**, **C** and **D**) and photomicrographs of their cross sections, with a magnification of 500 and 1000× (scale bar = 10 μm; 20 kV)

colorless, transparent, and shiny (Fig. 3A–D), consistent with the observations of Mali et al. [68]. The films were smooth, free of lumps, and without the formation of areas of phase separation. The films could be easily removed from the molds, and remained intact and flexible throughout the handling.

Photomicrograph images of the cross sections of the films were obtained to allow microstructural analysis and to assess the integrity and continuity of the films, a parameter required for the mechanical strength and barrier properties for use as wound dressings [69]. According to the photomicrograph images (Fig. 3 A1 and A2, B1 and B2, C1 and C2, and D1 and D2), the microstructure was shown to be homogeneous, with no evidence of coarse phase separation between ESRT and PVA, indicative of structural integrity and good mechanical properties of the films [65]. Similar results were reported by Maiti, Ray, Mitra, Sengupta, and Kar [70] and Priya, Gupta, Pathania, and Singha [71] for PVA/starch films prepared using the solvent casting technique, attributable to good compatibility between the polymers.

The interactions between the polymers in the mixtures influence the microstructural characteristics of the films, which, in turn, determine their functionality. FTIR analysis was performed to investigate the existence of specific interactions between the functional groups of PVA and the extract, by observing the displacement of specific IR bands, since groups of starch and PVA chains can form hydrogen bonds, as reported by Ramaraj [72].

The FTIR spectrum of ESRT (data not shown) exhibited characteristic peaks of starch-type polysaccharides [25, 57, 73, 74]. The band at 3285 cm^{-1} was assigned to the O–H stretching band. The broad signals at this band are due to intra-and/or intermolecular hydrogen bonds of the alcoholic function. Bands in the region of 2927 cm^{-1} were associated with the C–H symmetric and asymmetric stretching of methylene groups. The related C–H bending band was recorded at 1337 cm^{-1}. The signal observed at 1644 cm^{-1} can be associated with the water absorption in the amorphous region of the starch granules. Other overlapped signals in the same region can be related to the axial C=C vibration and N–H bending of amino derivatives owed to the presence of polypeptides in ESRT. Bands between 1700 and 1600 cm^{-1} are known as amide I and are mainly due to the C=O stretching of the peptide [75]. A C–N stretching band from other components of the extract was observed at 1151 cm^{-1}. The C–O–H bending vibration was observed at 1077 cm^{-1}, while its corresponding C–O stretching was observed at 1013 cm^{-1}. A=C–H bending vibration was observed at 929 cm^{-1}. Moreover, the signal at 861 cm^{-1} was ascribable to C–C stretching and that at 766 cm^{-1} was assigned to the N–H wagging. According to the literature, the bands at 1047 cm^{-1} and 1018 cm^{-1} have been assigned to an ordered and amorphous structure of starch [50, 73].

The FTIR spectrum of PVA (data not shown) presented a broader peak at 3275 cm^{-1}, observed for the stretching vibration of O–H moieties. Hydrogen bonding occurs between PVA chains due to high hydrophilic forces, which leads to broadening of this band. Alkyl stretching bands of PVA were observed at 2940 cm^{-1} and 2910 cm^{-1}. The C–H bending of the methylene and methine groups was detected at 1418 cm^{-1} and 1319 cm^{-1}, respectively. The C-H wagging occurs at approximately 1235 cm^{-1}. Bands of axial vibration of C–O occurred around

1089–1044 cm^{-1}, while the C–O–H stretching band was assigned at 917 cm^{-1}. The band near 1415 cm^{-1} can be attributed to the C–H of CH$_2$ from the residual acetate groups in PVA, which were remained after manufacturing of PVA from polyvinyl acetate by hydrolysis [77–79].

The FTIR spectra of PVA/ESRT films prepared in all the proportions displayed the same bands for the ESRT and PVA films (Fig. 4), with small displacements and changes in intensity, which can be correlated to their combined presence and the existence of some degree of interaction between the materials. According to Mansur et al. [84] and Reis et al. [79], the FTIR band at 1142 cm^{-1} has been used as an assessment tool for the semicrystalline structure of PVA and this band has been observed in the FTIR spectra of the films for all blends. Jayasekara et al. [57], Santos et al. [76], and Waghmare et al. [25] prepared films containing PVA and different types of starch, using glycerol as a plasticizer, and observed spectra similar to those found in the present study.

The crystalline structure of the films was investigated using XRD. All diffractograms were similar (Fig. 5). PVA is organized in a semicrystalline structure, presenting two crystalline planes, with signals at 11.5° and 19.8° [80]. In the present work, the diffractogram of the pure PVA film (data not shown) showed four peaks: 11.5°, 19.8°, 22.9°, and 40.4°. With respect to the PVA film with glycerol, there is the presence of an intense peak at 20.5° along with two peaks of low intensity at 23.4° and 41.3°, the first being associated with one of the semicrystalline phases of PVA. The weak peak at 11.5° was not observed, probably due to the change in the crystallinity of PVA by adding glycerol that resulted in physical interactions between the –OH groups of the chains.

The diffraction patterns displayed signals from both components of the PVA/ESRT films; however, a predominance of PVA signals was observed in all
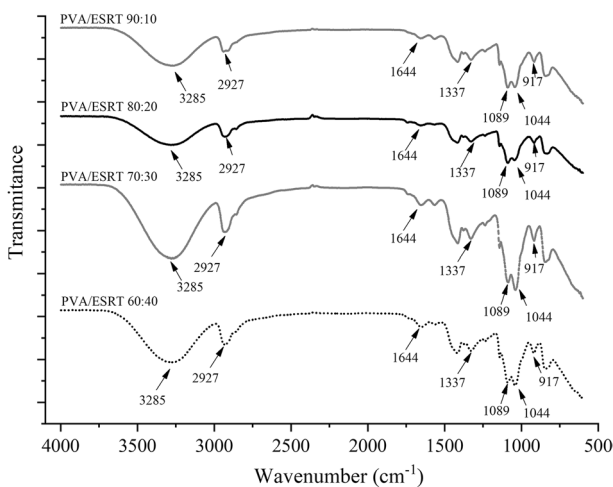

Fig. 4 FTIR-ATR spectra of films prepared from PVA/ESRT blends
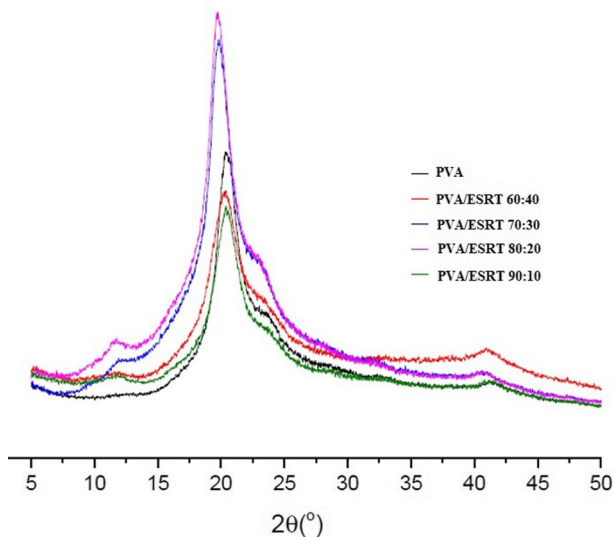
Fig. 5 X-ray diffractograms of PVA/ESRT films

diffractograms. The diffractometer profiles for the PVA/starch films in the present study were in line with the studies by Zanela et al. [81] and Zanela et al. [82]. According to the studies by Das et al. [83] and Popescu et al. [80], the PVA signal at 19.8° is attributed to the ordered arrangement of PVA molecules; however, it overlaps with the starch signals between 17° and 23.5°, indicating that the crystallinity of the mixtures depends mainly on the structure of the PVA. Popescu et al. [80] reported that an increase in the starch content in the blends could lead to an increase in signal intensity and a reduction in crystallinity in the films, which was attributed to the formation of hydrogen bonds between starch and PVA. In the present study, in the diffractograms of the films containing 30 and 20% w/w of starch, peaks were shifted from 20.5° to 19.8°; in addition, the signals observed at 11.5° and 12° were more intense. These findings suggest that an optimum concentration of starch in the blends may show interference in the crystalline structure of PVA. These findings are suggestive of partial miscibility and good compatibility between the materials.

The DSC and TG/DTG curves recorded for the ESRT and PVA films with glycerol and taro extract are shown in Fig. 6, Panel A and Panel B, respectively. According to the described method, preliminary heating was carried out to eliminate the thermal history of the sample (1st heating), followed by cooling and heating again (2nd heating). For the 90:10% w/w blend film, the crystallization temperature (Tc) was observed equal to that of pure PVA.

The DSC curves obtained after the first cooling showed a notable reduction in the crystallization temperature for the blends of the films containing 20, 30 and 40% w/w ESRT; the degree of reduction increased as a function of the decrease of ESRT proportion in the mixture. The DSC curves of the second heating demonstrated the existence of only one melting temperature for all blends, which was lower than that observed for the PVA film with plasticizer, indicative of the
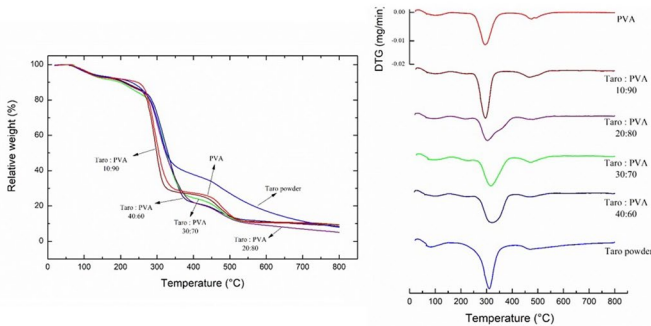
Panel **A**
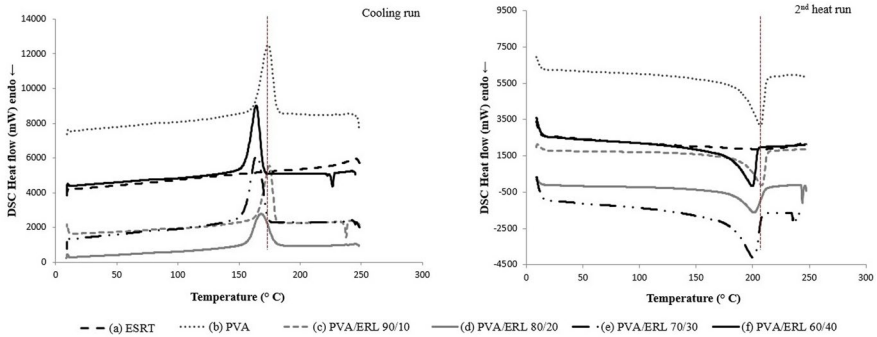
Panel **B**

Fig. 6 Panel **A**: DSC (cooling and second heating) curves for the PVA/ESRT films with 100:0, 90:10, 80:20, 70:30, and 60:40% w/w blends. Panel **B**: TG/DTG thermograms for taro extract, PVA film and PVA/ESRT films

formation of homogeneous mixtures. For the PVA films without ESRT, melting occurred at 208 °C, which is consistent with that reported for PVA/glycerol films in the literature. The present study demonstrated the same melting temperature (Tm) for the 90:10% w/w blend film as that for PVA without ESRT. However, regarding other blends, Tm was reduced to approximately 198 °C. These findings indicate that the presence of ESRT in the films leads to disorganization of the chains with decreased crystallinity, resulting from the formation of hydrogen bonds between starch and the hydroxyl groups of the PVA chains, reducing the melting temperature. It has been reported in the literature that the melting temperature of the mixture reduces further if there is good miscibility between the polymers [85–87]. Zhou et al. [88] obtained similar results, with a reduction in glass transition temperature (Tg) and melting temperature (Tm) for the films prepared with higher proportions of corn starch in the blends. According to Tian et al. [89], an increase in the proportion of corn starch in blends with PVA reduces the crystallinity of the synthetic polymer. The DSC results are in agreement with the FTIR and XRD analyses and indicated partial miscibility between the components.

Thermogravimetric methods also are used to study the miscibility and thermal stability behavior of polymeric systems by monitoring the mass loss of the sample in an inert atmosphere as a function of temperature [90]. Nonetheless, there are no data available in the literature regarding the thermal degradation profile of taro rhizome extract, except few reports on the degradation of granular or gelatinized taro starch.

The thermogram of the pure ESRT (Fig. 6; Panel B) showed three thermal degradation events. The first is related to water loss (Tpeak at approximately 80.8 °C), and the other two events, with maximum temperatures near 311 °C and 473 °C, were corresponding to the thermal degradation of the sample in two stages. All these events are characteristic of starch thermograms [23, 91]. The degradation observed in the second stage (Tpeak 311 °C; loss of mass 60.7%) can be associated with the breakdown of the starch chains with elimination of CO and CO_2, and formation of carbon residues. Zhang et al. [92] obtained corn starch thermograms similar to that of the present study, with the degradation event in the second stage with Tpeak near 316 °C and loss of mass 69%. In the case of the PVA films, in addition to water loss (Tpeak near 101 °C), two other degradation events could be observed, with Tpeak at 294 °C and near 476 °C, corresponding to the elimination of low molar masses as a result of the breakdown of the polymeric carbon chains accompanied with elimination of hydroxyl groups in dehydration reactions, and thermal decomposition of high molar mass polyenes derived from the first stage of degradation, respectively. Such findings are consistent with those in the literature [93, 94].

The TG and DTG thermograms of the films prepared with different proportions of PVA and ESRT presented three stages of degradation, with profiles similar to those previously analyzed. The first stage could be attributed to the evaporation of water and volatilization of easily degradable components; the second stage was corresponding to the characteristic degradation of the carbon–carbon chains, and the third stage represented the breakdown of the components with lower molar mass [88].

The formation of the blend between PVA and the ESRT led to a small displacement in the maximum temperature to a lower value from 101 °C to near 94 °C, referring to the first stage when compared to that of the pure PVA film; however, the maximum degradation temperature of the material in the second stage increased from 294 °C (pure PVA film) to approximately 322 °C (film prepared with 40% *w/w* ESRT), with a progressive increase related to the proportion of the ESRT in the mix. The loss of mass in the films obtained from the blends was approximately 7% less than that of the pure PVA film. These results of increase in the maximum degradation temperature and decrease in the fraction of mass lost indicated that the incorporation of the ESRT favored the thermal stabilization of the material. These data are consistent with those found in the literature [95]. Zhou et al. [88] observed that the PVA films and corn starch/PVA blends exhibited a three-step degradation pattern, similar to those found in this study. According to the authors, the addition of corn starch improved the thermal stability of PVA, since the activation energy for the main degradation (second stage) was higher than that of pure PVA. According to Jain et al. [96], an increase in thermal stability was observed in potato starch/PVA blends, with maximum stability for those containing 10% w/w of the natural

polymer. On the contrary, Othman et al. [90] observed reduction in the maximum degradation temperature of the films with an increase in the proportion of the natural polymer despite miscibility of the components of corn starch/PVA blends, indicating the existence of less thermal stability in the systems.

The evaluation of the thermal analysis results concluded that the blends formed were partially miscible and had improved thermal stability owing to an increase in the melting temperature and a reduction in mass loss compared to the PVA films without ESRT. The partial miscibility and the increase in thermal stability can be explained by the interactions between the − OH groups of PVA and the starch present in the ESRT [89]. These findings corroborate the visual and SEM observations, which showed the absence of coarse phase separation and domain formation in the films, and the films remained intact throughout handling. The analysis diffractometer profiles and glass transition temperature values indicated the changes in the crystallinity of PVA and films prepared with different proportions of the ESRT, suggesting the existence of compatibility and partial miscibility between PVA and the extract components.

Study of the barrier properties of films

Hydrophilicity and dissolution rate of the films are the main factors affecting the use of blends of PVA and natural polymers as wound dressings [89, 97]. Apparently, the functionality of the films is related to their wettability, degree of swelling and solubilization, thickness, and permeability to water vapor and other gases. The values of these parameters are listed in Table 2.

The films prepared from blends of the ESRT extract and PVA showed different barrier properties compared to those of the pure PVA films. The first parameter studied was the wettability of the films, which indicates the ability of a surface to be wetted by a liquid and can be defined as a surface/liquid interface phenomenon involving molecular interactions, and can be measured by the contact angle (θ). Hydrophilicity is wettability of a substance by water [98]. Several properties of biomaterials, such as water absorption, bioadhesion, and cellular interaction, are affected by wettability. It has been shown that cells adhere and spread more efficiently on the surfaces with adequate hydrophilicity compared to hydrophobic or very hydrophilic surfaces.

Studies have shown that moderately wettable surfaces provide strong cell–substrate and cell–cell interactions that induce better tissue regeneration [99]. The surface is considered as wet at $\theta < 30°$, partially wet at $30° < \theta < 90°$, negligibly wet at $\theta \geq 90°$, and not wet at $\theta \geq 180°$ [100]. All films exhibited partially wettable behavior in the SPB buffer, with θ between 34° and 60°. The contact angle observed for the PVA film is comparable with that observed in the literature for PVA/glycerol mixtures [101]. However, an incorporation of higher proportions of the ESRT in the blends resulted in reduced wettability by the liquid under study and increased contact angles, which can be justified by the increase in the formation of inter and intramolecular hydrogen bonds between the –OH groups in the PVA/ESRT films, similar

Table 2 Values of the contact angle (θ), swelling index (Q), loss of mass (ML), thickness, moisture content, and water vapor permeability rate observed for the films

Samples	θ (degrees) (10°s)	Q (%) (60°min)	ML (%) (48°h)	Moisture content (%) (105 °C)	Thickness (mm)	WVPR (g m^{-2}/d)
PVA	36.93 (±4.72)	90.64 (±4.46)	− 15.44 (±0.11)	8.45 (±1.38)	0.151 (±0.029)	414.91 (±85.98)
PVA/ESRT 9:1	34.47 (±3.22)	93.16 (±3.89)	− 14.55 (±0.50)	6.85 (±0.98)	0.151 (±0.032)	455.04 (±83.19)
PVA/ESRT 8:2	41.64 (±6.68)	93.05 (±6.13)	− 18.27 (±1.71)	6.25 (±0.74)	0.125 (±0.029)	636.27 (±71.08)
PVA/ESRT 7:3	42.48 (±3.38)	105.64 (±8.72)	− 21.20 (±0.63)	9.83 (±0.33)	0.118 (±0.020)	501.73 (±7.51)
PVA/ESRT 6:4	59.23 (±1.33)	108.35 (±4.24)	− 17.33 (±0.50)	8.67 (±0.04)	0.100 (±0.011)	730.30 (±117.08)

to the data obtained in the DSC and TG/DTG analyses. Such interactions are present as -OH free on the surface of the film available to interact with the wetting liquid.

In addition to contact angle, spreading (S) and work of adhesion (AW) are the parameters indicative of the affinity between a surface and a liquid. The spreading provides a measure of the difference between the cohesive force present in the liquid and the adhesion force between the surface and the liquid. When AW is more than the cohesive force, the value of S is positive, and the solid is completely dispersed in the liquid. When the cohesion force exceeds the work of adhesion, the S value is negative, resulting in partial spreading of the liquid on the solid surface. Higher value of the work of adhesion and, consequently, less spreadability are observed on more hydrophilic surfaces [102]. The obtained AW and S values followed the same trend as that observed for the contact angle in the present study.

Another important and considerable parameter is the thickness of the films, since it influences the swelling rate, solubilization, and water vapor permeability rate of the prepared films [103]. It was observed that the increase in the ESRT content in the blends caused a decrease in the thickness of the films. This reduction can be correlated with the packaging of polymer chains in the films due to the formation of hydrogen bonds between the -OH groups of PVA and the starch present in the extract.

The residual moisture content of the films ranged from 6.25 to 9.83%. The swelling index (Q%) is related to the amount of water absorbed by the film *versus* dry weight of the film when immersed in the study medium for a certain time. Swelling index influences the capacity of absorption of fluids and exudates by the film, which is essential for controlling the moisture in the wound, favoring tissue regeneration. The ideal swelling index for dressings depends mainly on the type and condition of the wound [99]. An increase in Q% was observed with an increase in the ESRT content in the blends, with films containing 30 and 40% w/w of the ESRT showing the highest values. The increase in swelling for blends richer in ESRT may be due to a reduction in the crystallinity of PVA, giving rise to a network structure that can hold a higher amount of water.

The solubility test quantifies the loss of mass of the films after immersing them in a liquid medium for 48 h [36]. This parameter is related to the affinity for water and the interaction between the constituent polymer chains. Although, as previously mentioned, an optimum degree of hydrophilicity of the films is desirable, high solubility results in material loss and film breakdown. The lower the solubility, the greater the possibility of maintaining the integrity of the film during use. In the present study, the solubility of the films ranged between 14.5 and 21.2%, with the film containing 30% w/w of the ESRT showing the highest loss of mass (21.2%). It was observed that the presence of the extract caused an increase in mass loss. Prerequisites for the loss of mass study are that it should be carried out over a long period of contact (48 h) and all films should have remained intact during the performance, which is a characteristic required for their use as dressings.

Water vapor permeability rate (WVPR) is another important property affecting the use of the films as wound dressings, as both accumulation and excessive loss of liquids can impair the healing process and tissue repair, warranting for an optimum moisture balance. Therefore, the production of a semipermeable dressing is

desirable [99]. Permeability is related to other parameters such as swelling index and thickness, because the films with greater swelling index will capture and permeate a higher amount of water vapors resulting in saturation. On the contrary, an increase in thickness decreases the WVPR [104]. The current study demonstrated an increase in permeability, with the highest WVPR obtained for the film containing 40% w/w of the ESRT (730.3 g m^{-2} day^{-1}). Moreover, the increase observed in the WVPR values was not proportional to the part of the ESRT in the blends, and can be explained by the reduced thickness and increased Q value of the films. Additionally, the highest permeability values were observed for thin films, which is in agreement with that reported in the literature. The rate of water vapor permeability for normal skin has been reported as 204 g m^{-2} day^{-1}. The WVPR measure for commercial dressings ranges from 139 to 10,973 g m^{-2} day^{-1}, depending on the materials used and application purposes [105].

The findings of the study of the barrier properties indicated changes to a greater extent in blends containing 20, 30 and 40% w/w of the ESRT, with respect to the parameters related to the residual moisture content after 60 min of contact, loss of mass after 48 h, and water vapor permeability rate after 24 h, which is beneficial for materials used in bioactive wound dressings. These results are attributable to the presence of greater interactions between the materials by hydrogen bonding. Notably, the films remained intact throughout handling and during all tests.

Mechanical properties

The mechanical properties of films are influenced by several factors, including film thickness, processing method, and test speed, which make it difficult to establish accurate comparisons between the results obtained in different studies [106, 107]. Table 3 provides the data obtained from the mechanical test of the films.

The findings of the mechanical test verify a trend of improved mechanical properties for the films containing the extract, with increase in all parameters studied, compared to the PVA film without ESRT. These results can be justified by the presence of a continuous and integral matrix by SEM findings, the existence of interactions between the polymers in the blend leading to changes in crystallinity by the FTIR, XRD, and DSC data, and the increase in the thermal stability of the films prepared from the blends by thermogravimetry analysis (TG/DTG) data.

Table 3 Tensile properties of PVA/glycerol and PVA/starch blend films

Samples	Tensile strength (MPa)	Tensile modulus (MPa)	Ultimate elongation (%)
PVA	50.44 (± 10.66)	434.75 (± 59.26)	90.75 (± 27.02)
PVA/ESRT 9:1	94.34 (± 1.68)	499.33 (± 44.84)	265.33 (± 16.80)
PVA/ESRT 8:2	97.45 (± 20.60)	696.50 (± 271.56)	203.12 (± 61.88)
PVA/ESRT 7:3	66.43 (± 16.79)	585.28 (± 129.92)	147.40 (± 27.33)
PVA/ESRT 6:4	70.40 (± 19.05)	711.50 (± 150.54)	132.95 (± 24.43)

According to Zhou et al. [88], strong interactions that occur between PVA and starch are favored by the presence of glycerol in the blends, resulting in greater tensile strength at break and improved elongation. Musa and Hameed [108] prepared PVA/starch films by the solvent casting method and observed the formation of clusters and empty spaces in the films, resulting in reduction in all mechanical strength parameters. However, unlike the present study, the authors reported that starch was incorporated directly in the freshly prepared PVA solution for preparing blends, without prior gelatinization. Therefore, it can be anticipated that the prior gelatinization of starch resulted in a colloidal dispersion, favoring the formation of a more homogeneous blend, which is reflected by the increase in mechanical properties besides the formation of a continuous microstructure.

Preliminary biocompatibility

The hemolysis index (%HI) is an indirect measure of biocompatibility that determines the degree of hemolysis in red blood cells when the material or device is placed in contact with the blood [109]. The hemolysis index for the pure PVA film was observed as 2.64% ($\pm 0.34\%$), whereas the values ranged from 1.98% ($\pm 0.15\%$) to 2.84% ($\pm 0.42\%$) for other films. According to Pal et al. [110], materials with a hemolysis index of less than 5% are considered as highly biocompatible. According to the classification of Kamoun et al. [109], the prepared films can be classified as slightly hemolytic ($2 < \%HI < 5$).

The effect of the films on the growth of cells was investigated using the cellular viability assay using different concentrations of the films; the cell viability was observed between 70% (1 mg ml^{-1}) and 90% (0.125 mg ml^{-1}) compared to the basal group (100%) (Fig. 7). The results showed that the films were non-cytotoxic and biocompatible, because the materials were considered cytotoxic if they reduced the viability of the cells by more than 50% [111]. There was no significant difference between the values obtained for the films prepared with different proportions
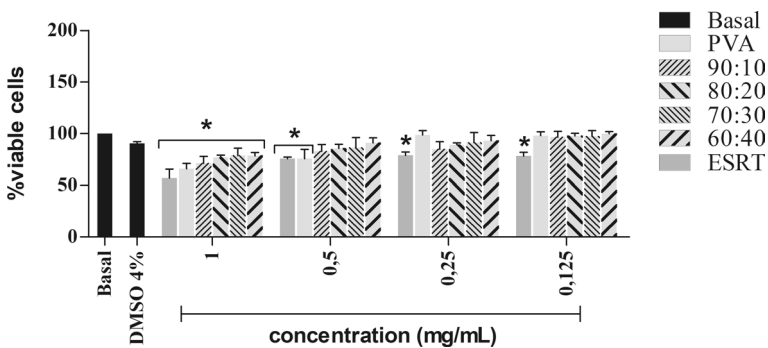

Fig. 7 Effect of different concentrations of films on viability of Raw 264.7 cells. *$p < 0.05$; comparison with the baseline group. Values are expressed as the mean $\pm$ SD of three independent experiments performed in triplicate

of the ESRT and PVA. These findings are in accordance with the literature that has reported PVA as a non-toxic and biocompatible polymer, and with taro rhizomes, which have reported antioxidant, proliferative and healing activity [17, 112, 113].

It is worth mentioning that the tested concentration of the extract in the films was lower than the concentration of the pure extract tested due to a limitation of the technique, since the film swells in contact with the liquid medium. For higher proportions of ERST in the films, the percentile of viable cells was higher than for pure PVA, mainly for the highest concentrations, despite the lack of significance when compared to the basal group. In agreement with the literature, in the present work, ESRT showed healing activity similar to the commercial product used as a healing agent and seems to improve cellular viability in the presence of PVA against Raw 264.7 cells.

Conclusion

Rhizomes from taro are a natural source of bioactive compounds and amylaceous polysaccharides. Crude extracts obtained from taro rhizomes acted positively on the closure of the lesions, with an ulcer healing index similar to that observed for the commercial product. The presence of starch in the extract, with a crystalline fraction (amylose) of 19%, was confirmed by the XRD analysis. In addition, prior gelatinization of the ESRT at 85 °C favored the formation of films by blends with PVA that presented a continuous and homogeneous microstructure, and without coarse phase separation as validated by the SEM. The interaction between PVA and the gelatinized starch in all blends with different PVA/ESRT proportions was identified by the DSC data. However, according to the TG/DTG data, there was an improvement in the thermal stability of the blends, as evidenced by the increase in the melting temperature and reduction in mass loss compared to the PVA films without ESRT. Moreover, the blends were partially miscible and had altered crystallinity compared to that of the pure PVA as observed by thermal analyses and XRD. Additionally, a greater degree of change in the parameters related to retention of saline buffer after 60 min, loss of mass after 48 h, and WVPR after 24 h was evident in the blend films containing 20, 30, and 40% w/w of starch, with disorganization of the crystalline chains due to the greater interactions between the materials; these results are in favor to use these materials to prepare bioactive wound dressings. Regarding the mechanical test, the results showed an improvement in the modulus of elasticity, tensile strength at break, and deformation during break for all blends compared to the pure polymer, corroborating the results obtained in the physicochemical characterization. Furthermore, the films showed good biocompatibility and were non-cytotoxic, indispensable properties for their use as bioactive dressings. Based on these findings, we conclude that the crude extract of taro rhizomes in high proportion with PVA has promising use as a biomaterial to prepare wound dressings.

Declarations

Conflict of interest The authors declare that they have no conflict of interest.

Consent for publication All authors give consent for publication.

Ethical approval *Ethics Committee on the Use of Animals* (ECUA-UFES): approval number 006/2019.

References

1. Babu RP, O'Connor K, Seeram R (2013) Current progress on bio-based polymers and their future trends. Prog Biomat 2:1–16
2. Bedor PBA, Caetano RMJ, Souza Júnior FG, Leite SGF (2020) Advances and perspectives in the use of polymers in the environmental area: a specific case of PBS in bioremediation. Polímeros 30:1–10
3. Jiang T, Duan Q, Zhu J, Liu H, Yu L (2020) Starch-based biodegradable materials: challenges and opportunities. Adv Ind Eng Polym Res 3:8–18
4. Choi G, Cha HJ (2019) Recent advances in the development of nature-derived photocrosslinkable biomaterials for 3D printing in tissue engineering. Biomater Res 23:18
5. Barua E, Deoghare AB, Deb P, Lala SD (2018) Naturally derived biomaterials for development of composite bone scaffold: a review. IOP Mat Sci Eng 377:012013
6. Souza JRCL, Villanova JCO, Souza TS, Maximino RC, Menini L (2021) Vegetable fixed oils obtained from soursop agro-industrial waste: extraction, characterization and preliminary evaluation of the functionality as pharmaceutical ingredients. Environ Technol Innov 21:101379
7. Jiménez A, Fabra MJ, Talens P, Chiralt A (2012) Edible and biodegradable starch films: a review. Food Biopro Tech 5:2058–2076
8. Abuajah CI, Ogbonna AC, Osuji CM (2015) Functional components and medicinal properties of food: a review. J Food Sci Technol 52:2522–2529
9. Ahmed A, Khan F (2013) Extraction of starch from taro (*Colocasia esculenta*) and evaluating it and further using taro starch as disintegrating agent in tablet formulation with over all evaluation. Inventi Rapid Novel Excip 2013:1–5
10. Assefa Z, Admassu S (2013) Development and characterization of antimicrobial packaging films. J Food Process Technol 4:235–241
11. Subhash CK, Sarla S, Jaybardhan S (2012) Phytochemical screening of garhwal himalaya wild edible tuber *Colocasia esculenta*. Int Res J Pharm 3:181–186
12. Mijinyawa AH, Durga G, Mishra A (2018) Isolation, characterization, and microwave assisted surface modification of *Colocasia esculenta* (L.) Schott mucilage by grafting polylactide. Int J Biol Macromol 119:1090–1097
13. Leong ACN, Kinjo Y, Tako M, Iwasaki H, Oku H, Tamaki H (2010) Flavonoid glycosides in the shoot system of Okinawa Taumu (*Colocasia esculenta* S.). Food Chem 119:630–635
14. Li H, Dong Z, Liu X, Chen H, Lai F, Zhang M (2018) Structure characterization of two novel polysaccharides from *Colocasia esculenta* (Taro) and a comparative study of their immunomodulatory activities. J Funct Foods 42:47–57

15. Pereira PR, Silva JT, Verícimo MA, Paschoalin VMF, Teixeira GAPB (2015) Crude extract from taro (*Colocasia esculenta*) as a natural source of bioactive proteins able to stimulate haematopoietic cells in two murine models. J Funct Foods 18:333–343

16. Simsek S, El SN (2015) In vitro starch digestibility, estimated glycemic index and antioxidant potential of taro (*Colocasia esculenta* L. Schott) corn. Food Chem 168:257–261

17. Gonçalves RF, Silva AMS, Silva AM, Valentão P, Ferreres F, Gil-Izquierdo A, Silva JB, Santos D, Andrade PB (2013) Influence of taro (*Colocasia esculenta* L. Shott) growth conditions on the phenolic composition and biological properties. Food Chem 141:3480–3485

18. Sharma P, Mishra NK (2009) Ethno-medicinal uses and agro-biodiversity of Barmana region in Bilaspur district of Himachal Pradesh, Northwestern Himalaya. Ethnobot Leaflets 5:709–721

19. Mukurumbira A, Mariano M, Dufresne A, Mellem JJ, Amonsou EO (2017) Microstructure, thermal properties and crystallinity of Amadumbe Starch nanocrystals. Int J Biol Macromol 102:241–247

20. Matveev YI, Grinberg VY, Tolstoguzov VB (2000) The plasticizing effect of water on proteins, polysaccharides and their mixtures. Glassy state of biopolymers. Food Seeds Food Hydrocoll 14:425–437

21. Yu L, Dean K, Li L (2006) Polymer blends and composites from renewable resources. Prog Polym Sci 31:576–602

22. Shah U, Gani A, Ashwar BA, Shah A, Ahmad M, Gani A, Wani IA, Masoodi FA (2015) A review of the recent advances in starch as active and nanocomposite packaging films. Cogent Food Agric 1:1115640

23. Andrade LA, Barbosa NA, Pereira J (2017) Extraction and properties of starches from the non-traditional vegetables yam and taro. Polímeros 27:151–157

24. Liporacci JSN, Mali S, Grossmann MVE (2005) Effects of extraction method on chemical composition and functional properties of yam starch (*dioscorea alata*). Semina Ciênc Agrár 26(3):345–352

25. Waghmare VS, Wadke PR, Dyawanapelly S, Deshpande A, Jain R, Dandekar P (2018) Starch based nanofibrous scaffolds for wound healing applications. Bioact Mater 3:255–266

26. Chukwu KI, Udeala OK (2000) Binding effectiveness of *Colocasia esculenta* Gum in poorly compressible drugs-paracetamol and metronidazole tablet formulations. Boll Chim Farm 139:89–97

27. Gurpreet A, Karan M, Inderbir S (2011) Formulation and evaluation of mucoadhesive matrix tablets of taro gum: optimization using response surface methodology. Polim Med 41:23–34

28. Soumya M, Chowdary YA, Swapna VN, Prathyusha ND, Geethika R, Jyostna B, Mohan KSK (2014) Preparation and optimization of sustained release matrix tablets of metoprolol succinate and taro gum using response surface methodology. Asian J Pharm 8:51–57

29. Pawar HA, Kamat SR (2017) Development and evaluation of mouth dissolving film of ondansetron hydrochloride using hpmc e5 in combination with taro gum and other commercially available gums. J Mol Pharm Org Process Res 5:138

30. Wardhani RAK, Asri LATW, Rachmawati H, Khairurrijal K, Purwasasmita BS (2020) Physical-chemical crosslinked electrospun *Colocasia esculenta* Tuber protein-chitosan-poly(ethylene oxide) nanofibers with antibacterial activity and cytocompatibility. Int J Nanomed 15:6433–6449

31. Caetano KS, Frade MAC, Minatel DG, Santana LA, Enwemeka CS (2009) Phototherapy improves healing of chronic venous ulcers. Photomed Laser Surg 27:111–118

32. Garros IC, Campos ACL, Tâmbara EM, Tenório SB, Torres OJM, Agulham MA, Araújo ACF, Santis-Isolan PMB, Oliveira RM, Arruda ECM (2006) Extract from passiflora edulis on the healing of open wounds in rats: morphometric and histological study. Acta Cir Bras 21:55–65

33. Koga AY, Pereira AV, Lipinski LC, Oliveira MRP (2018) Evaluation of wound healing effect of alginate films containing aloe vera (*Aloe barbadensis* Miller) gel. J Biomater Appl 32:1212–1221

34. Zonari A, Martins TMM, Paula ACC, Boeloni JN, Novikoff S, Marques AP, Correlo VM, Reis RL, Goes AM (2015) Polyhydroxybutyrate-co-hydroxyvalerate structures loaded with adipose stem cells promote skin healing with reduced scarring. Acta Biomater 17:170–181

35. Xie L, Jiang M, Dong X, Bai X, Tong J, Zhou J (2012) Controlled mechanical and swelling properties of poly (vinyl alcohol)/sodium alginate blend hydrogels prepared by freeze-thaw followed by ca^{2+} crosslinking. J Appl Polym Sci 124:823–831

36. Flores SK, Costa D, Yamashita F, Gerschenson LN, Grossmann MV (2010) Mixture design for evaluation of potassium sorbate and xanthan gum effect on properties of tapioca starch films obtained by extrusion. Mater Sci Eng C Mater Biol Appl 30:196–202

37. ASTM. American Society for Testing and Materials (2005) Standard Test Method for Water Vapor Transmission of Materials. ASTM E 96–05. ASTM, Philadelphia

38. Mosmann T (1983) Rapid colorimetric assay for cellular growth and survival: application to proliferation and cytotoxicity assays. J Immunol Methods 65:55–63

39. Kamiloglu S, Toydemir G, Boyacioglu D, Beekwilder J, Hall RD, Capanoglu E (2016) A review on the effect of drying on antioxidant potential of fruits and vegetables. Crit Rev Food Sci Nutr 56:S110–S129

40. Craig D (1999) The relevance of the amorphous state to pharmaceutical dosage forms: glassy drugs and freeze dried systems. Int J Pharm 179(2):179–207

41. Wang X, Reddy CK, Xu B (2018) A systematic comparative study on morphological, crystallinity, pasting, thermal and functional characteristics of starches resources utilized in China. Food Chem 259:81–88

42. Sajilata MG, Singhal R, Kulkarni PR (2006) Resistant starch—a review. Compr Rev Food Sci Food Saf 5:1–17

43. Campos CA, Gerschenson LN, Flores SK (2011) Development of edible films and coatings with antimicrobial activity. Food Bioprocess Technol 4:849–875

44. Liao LS, Liu HS, Liu XX, Chen L, Yu L, Chen P (2014) Development of microstructures and phase transitions of starch. Acta Polym Sin 2014:761–773

45. Xie F, Halley PJ, Avérous L (2012) Rheology to understand and optimize processibility, structures and properties of starch polymeric materials. Prog Polym Sci 37:595–623

46. Yu L, Christie G (2005) Microstructure and mechanical properties of orientated thermoplastic starches. J Mater Sci 40:111–116

47. Bertuzzi MA, Gottifredi JC, Armada M (2012) Mechanical properties of a high amylose content corn starch based film, gelatinized at low temperature. Braz J Food Technol 15:219–227

48. Dome K, Podgorbunskikh E, Bychkov LO (2020) Changes in the crystallinity degree of starch having different types of crystal structure after mechanical pretreatment. Polymers 12:641

49. Frost K, Kaminski D, Kirwan G, Lascaris E, Shanks R (2009) Crystallinity and structure of starch using wide angle X-ray scattering. Carbohydr Polym 78:543–548

50. Lopez-Rubio A, Flanagan BM, Shrestha AK, Gidley MJ, Gilbert EP (2008) Molecular rearrangement of starch during in vitro digestion: toward a better understanding of enzyme resistant starch formation in processed starches. Biomacromol 9(7):1951–1958

51. Singh V, Ali SZ, Somashekar R, Mukherjee PS (2006) Nature of crystallinity in native and acid modified starches. Int J Food Prop 9:845–854

52. Aboubakar NYN, Scher J, Mbofung CMF (2008) Physicochemical, thermal properties and microstructure of six varieties of taro (*Colocasia escule*nta L. Schott) flours and starches. J Food Eng 86:294–305

53. Sit N, Misra S, Baruah D, Badwaik LS, Deka SC (2014) Physicochemical properties of taro and maize starch and their effect on texture, colour and sensory quality of tomato ketchup. Starch 66:294–302

54. Sukhija S, Singh S, Riar CS (2016) Isolation of starches from different tubers and study of their physicochemical, thermal, rheological and morphological characteristics. Starch 68:160–168

55. Pereira PR, Del Aguila EM, Verícimo MA, Zingali RB, Paschoalin VMF, Silva JT (2014) Purification and characterization of the lectin from taro (*Colocasia esculenta*) and its effect on mouse splenocyte proliferation in vitro and in vivo. Protein J 33:92–99

56. Swarnkar S, Katewa SS (2008) Ethnobotanical observation on tuberous plants from tribal area of Rajasthan (India). Ethnobot Leaflets 2008(1):87

57. Jayasekara R, Harding I, Bowater I, Christie GBY, Lonergan GT (2004) Preparation, surface modification and characterisation of solution cast starch pva blended films. Polym Test 23:17–27

58. López OV, García MA, Zaritzky NE (2008) Film forming capacity of chemically modified corn starches. Carbohydr Polym 73:573–581

59. Paes SS, Yakimets I, Mitchell JR (2008) Influence of gelatinization process on functional properties of cassava starch films. Food Hydrocoll 22:788–797

60. Hoover R, Ratnayake WS (2001) Determination of total amylose content of starch. Curr Protoc Food Anal Chem 00:1–5

61. Liu H, Xie F, Yu L, Chen L, Li L (2009) Thermal processing of starch-based polymers. Prog Polym Sci 34:1348–1368

62. Chen P, Yu L, Simon GP, Liu X, Dean K, Chen L (2011) Internal structures and phase-transitions of starch granules during gelatinization. Carbohyd Polym 83:1975–1983

63. Zhong F, Li Y, Ibáñez AM, Oh MH, McKenzie KS, Shoemaker C (2009) The effect of rice variety and starch isolation method on the pasting and rheological properties of rice starch pastes. Food Hydrocoll 23:406–414

64. Araujo-Farro PC, Podadera G, Sobral PJA, Menegalli FC (2010) Development of films based on quinoa (*Chenopodium quinoa*, Willdenow) starch. Carbohydr Polym 81:839–848

65. Mali S, Grossmann MVE, Garcia MA, Martino MN, Zaritzky NE (2002) Microstructural characterization of yam starch films. Carbohydr Polym 50:379–386

66. García MA, Martino MN, Zaritzky NE (2000) Microstructural characterization of plasticized starch-based films. Starch 52:118–124

67. Sothornvit R, Krochta JM (2001) Plasticizer effect on mechanical properties of *β*-lactoglobulin films. J Food Eng 50:149–155

68. Mali S, Grossmann MVE, García MA, Martino MN, Zaritzky NE (2004) Barrier, mechanical and optical properties of plasticized yam starch films. Carbohydr Polym 56(2):129–135

69. El Sayed AM, El-Gamal S, Morsi WM, Mohammed G (2015) Effect of PVA and copper oxide nanoparticles on the structural, optical, and electrical properties of carboxymethyl cellulose films. J Mater Sci 50:4717–4728

70. Maiti S, Ray D, Mitra D, Sengupta S, Kar T (2011) Structural changes of starch/polyvinyl alcohol biocomposite films reinforced with microcrystalline cellulose due to biodegradation in simulated aerobic compost environment. J Appl Polym Sci 122:2503–2511

71. Priya B, Gupta VK, Pathania D, Singha AS (2014) Synthesis, characterization and antibacterial activity of biodegradable starch/PVA composite films reinforced with cellulosic fibre. Carbohydr Polym 109:171–179

72. Ramaraj B (2007) Crosslinked poly(vinyl alcohol) and starch composite films. II. physicomechanical, thermal properties and swelling studies. J Appl Polym Sci 103:909–916

73. Liu TY, Ma Y, Yu SF, Shi J, Xue S (2011) The effect of ball milling treatment on structure and porosity of maize starch granule. Inno Food Sci Emerg Technol 12:586–593

74. Sarwar MS, Niazi MBK, Jahan Z, Ahmad T, Hussain A (2018) Preparation and characterization of PVA/nanocellulose/ag nanocomposite films for antimicrobial food packaging. Carbohydr Polym 184:453–464

75. Andrade LA, Nunes CA, Pereira J (2015) Relationship between the chemical components of taro rhizome mucilage and its emulsifying property. Food Chem 178:331–338

76. Santos C, Silva CJ, Büttel Z, Guimarães R, Pereira SB, Tamagnini P, Zille A (2014) Preparation and characterization of polysaccharides/PVA blend nanofibrous membranes by electrospinning method. Carbohydr Polym 99:584–592

77. Kharazmi A, Faraji N, Hussin RM, Saion E, Yunus WMM, Behzad K (2015) Structural, optical, opto-thermal and thermal properties of zns-pva nanofluids synthesized through a radiolytic approach. Beilstein J Nanotechnol 6:529–536

78. Mansur HS, Oréfice RL, Mansur AAP (2004) Characterization of poly(vinyl alcohol)/poly(ethylene glycol) hydrogels and pva-derived hybrids by small-angle x-ray scattering and ftir spectroscopy. Polymer 45:7193–7202

79. Reis EF, Campos FS, Lage AP, Leite RC, Heneine LG, Vasconcelos WL, Lobato ZIP, Mansur HS (2006) Synthesis and characterization of poly(vinyl alcohol) hydrogels and hybrids for rmpb70 protein adsorption. Mat Res 9:185–191

80. Popescu MC, Dogaru BI, Goanta M, Timpu D (2018) Structural and morphological evaluation of cnc reinforced pva/starch biodegradable films. Int J Biol Macromol 116:385–393

81. Zanela J, Shirai MA, Reis MO, Mali S, Grossmann MVE, Yamashita F (2015) Mixture design to develop biodegradable sheets with high levels of starch and polyvinyl alcohol. Starch 67:1011–1019

82. Zanela J, Bilck AP, Casagrande M, Grossmann MVE, Yamashita F (2018) Polyvinyl alcohol (PVA) molecular weight and extrusion temperature in starch/pva biodegradable sheets. Polímeros 28:256–265

83. Das K, Ray D, Bandyopadhyay NR, Gupta A, Sengupta S, Sahoo S, Mohanty A, Misra M (2010) Preparation and characterization of cross-linked starch/poly(vinyl alcohol) green films with low moisture absorption. Ind Eng Chem Res 49(5):2176–2185

84. Mansur HS, Sadahira CM, Souza AN, Mansur AAP (2008) FTIR spectroscopy characterization of poly(vinyl alcohol) hydrogel with different hydrolysis degree and chemically crosslinked with glutaraldehyde. Mater Sci Eng C Mater Biol Appl 28(4):539–548

85. Orts WJ, Nobes GAR, Glenn GM, Gray GM, Imam S, Chiou BS (2007) Blends of starch with ethylene vinyl alcohol copolymers: effect of water, glycerol, and amino acids as plasticizers. Polym Adv Technol 18(8):629–635

86. Sreekumar PA, Al-Harthi MA, De SK (2012) Effect of glycerol on thermal and mechanical properties of polyvinyl alcohol/starch blends. J Appl Polym Sci 123(1):135–142

87. Thakore IM, Desai S, Sarawade BD, Devi S (2001) Studies on biodegradablility, morphology and thermo-mechanical properties of ldpe/modified starch blends. Eur Polym J 37(1):151–160

88. Zhou XYY, Cui YF, Jia DM, Xie D (2009) Effect of a complex plasticizer on the structure and properties of the thermoplastic pva/starch blends. Polym Plast Tech Eng 48(5):489–495

89. Tian H, Yan JA, Rajulu AV, Xiang A, Luo X (2017) Fabrication and properties of polyvinyl alcohol/starch blend films: effect of composition and humidity. Int J Biol Macromol 96:518–523

90. Othman N, Azahari NA, Ismail H (2011) Thermal properties of polyvinyl alcohol (pvoh)/corn starch blend film. Malays Polym J 6:147–154

91. Zhang M, Cheng Z, Zhao T, Liu M, Hu M, Li J (2014) Synthesis, characterization, and swelling behaviors of salt-sensitive maize bran-poly(acrylic acid) superabsorbent hydrogel. J Agric Food Chem 62:8867–8874

92. Zhang R, Wang X, Cheng M (2018) Preparation and characterization of potato starch film with various size of Nano-Sio$_2$. Polymers 10:1172

93. Cassu SN, Felisberti MI (2005) Dynamic mechanical behavior and relaxations in polymers and polymeric blends. Quim Nova 28:255–263

94. Costa NN, Lopes LF, Ferreira DF, Prado EML, Severi JA, Resende JA, Careta FP, Pimentel MC, Carreira LG, Cotrim SSOL, OreficeVillanova MAPRLJCO (2020) Polymeric films containing pomegranate peel extract based on pva/starch/paa blends for use as wound dressing: in vitro analysis and physicochemical evaluation. Mater Sci Eng C Mater Biol Appl 109:110643

95. Athawale VD, Lele V (2000) Thermal studies on granular maize starch and its graft copolymers with vinyl monomers. Starch 52:205–213

96. Jain N, Singh VK, Chauhan S (2018) Dynamic and creep analysis of polyvinyl alcohol based films blended with starch and protein. J Polym Eng 39:35–47

97. Jayakumar R, Prabaharan M, Kumar PTS, Nair SV, Tamura H (2011) Biomaterials based on chitin and chitosan in wound dressing applications. Biotech Adv 29:322–337

98. Dutra JAP, Carvalho SG, Zampirolli ACD, Daltoé RD, Teixeira RM, Careta FP, Cotrim MAP, Orefice RL, Villanova JCO (2017) Papain wound dressings obtained from poly(vinyl alcohol)/calcium alginate blends as new pharmaceutical dosage form: preparation and preliminary evaluation. Eur J Pharm Biopharm 113:11–23

99. Güneş S, Tıhmınlıoğlu F (2017) *Hypericum perforatum* incorporated chitosan films as potential bioactive wound dressing material. Int J Biol Macromol 102:933–943

100. Karbowiak T, Debeaufort F, Voilley A (2006) Importance of surface tension characterization for food, pharmaceutical and packaging products: a review. Crit Rev Food Sci Nut 46:391–407

101. Salleh MSN, Nor NNM, Mohd N (1809) Draman SFS (2017) water resistance and thermal properties of polyvinyl alcohol-starch fiber blend film. AIP Conf Proc 1:020045

102. Sriamornsak P, Wattanakorn N, Nunthanid J, Puttipipatkhachorn S (2008) Mucoadhesion of pectin as evidence by wettability and chain interpenetration. Carbohydr Polym 74:458–467

103. Galdeano MC, Wilhelm AE, Mali S, Grossmann MVE (2013) Influence of thickness on properties of plasticized oat starch films. Braz Arc Biol Technol 56:637–644

104. Hu Y, Topolkaraev V, Hiltner A, Baer E (2001) Measurement of water vapor transmission rate in highly permeable films. J Appl Polym Sci 81:1624–1633

105. Sood A, Granick MS, Tomaselli NL (2014) Wound dressings and comparative effectiveness data. Adv Wound Care 3:511–529

106. Domene-López D, Guillén MM, Martin-Gullon I, García-Quesada JC, Montalbán MG (2018) Study of the behavior of biodegradable starch/polyvinyl alcohol/rosin blends. Carbohydr Polym 202:299–305

107. Souza AC, Benze R, Ferrão ES, Ditchfield C, Coelho ACV, Tadini CC (2012) Cassava starch biodegradable films: influence of glycerol and clay nanoparticles content on tensile and barrier properties and glass transition temperature. LWT-Food Sci Technol 46:110–117

108. Musa BH, Hameed NJ (2020) Study of the mechanical properties of polyvinyl alcohol/starch blends. Mater Today Proc 20:439–442

109. Kamoun EA, Kenawy ERS, Chen X (2017) A review on polymeric hydrogel membranes for wound dressing applications: pva-based hydrogel dressings. J Adv Res 8:217–233

110. Pal K, Banthia AK, Majumdar DK (2009) Polymeric hydrogels: characterization and biomedical applications. Des Monom Polym 12:197–220

111. OECD 439 (2019) Test no. 439: In vitro skin irritation: reconstructed human epidermis test method. in Oecd guidelines for the testing of chemicals, Section4: Health Effects

112. Alexandre N, Ribeiro J, Gärtner A, Pereira T, Amorim I, Fragoso J, Lopes A, Fernandes J, Santos JD, Maurício AC (2014) Biocompatibility and hemocompatibility of polyvinyl alcohol hydrogel used for vascular grafting - in vitro and in vivo studies. J Biom Mat Res Part A 102:4262–4275

113. Muppalaneni S, Omidian H (2013) Polyvinyl alcohol in medicine and pharmacy: a perspective. J Dev Drugs 2:1–5

Publisher's Note Springer Nature remains neutral with regard to jurisdictional claims in published maps and institutional affiliations.